

Thouless pumps and universal geometry-induced drift velocity in multi-sliding quasi-periodic lattices

Zixun Xu¹ and Yuan Yao^{1,*}

¹*Institute of Condensed Matter Physics, School of Physics and Astronomy,
Shanghai Jiao Tong University, Shanghai 200240, China*

(Dated: December 3, 2025)

Quantized Thouless pumps in periodic systems, set by Chern numbers or Wannier-center winding, is by now fairly well established, whereas its quasi-periodic extensions still require further clarification. Here, we develop a general quantitative paradigm for bulk Thouless pumps in continuous models with spacetime quasi-periodicity, applicable to arbitrary spatial dimensions. Within this framework, the bulk pumping turns out to be governed by an emergent long wave-length effective potential. Based on this mechanism, we obtain our main result a universal relation between topological drifting and the geometry of quasi Brillouin zone. Reduced to periodic systems, our result gives an explicit and compact formula which enables us to directly calculate Chern numbers by microscopic data. These proposals are corroborated by simulations of one- and two-dimensional continuous moiré-type spacetime quasi-periodic lattices, which exhibit stable, localized, directional drift in excellent agreement with the theory.

Introduction— Classifying and recognizing various phases of quantum phases is a central issue in statistical and condensed matter physics. Characterizations of gapped quantum phases by various quantized responses, so-called topological invariants, have attracted great efforts. Thouless pumps [1], as the dynamical analogue of the typical quantum Hall effect [2], are canonical examples of quantized transport: during each adiabatic cycle, the charge transferred across the system corresponds to a topological invariant—the Chern number that is robust against local perturbations, inspiring broad interest as a proper realization of novel current standards [3, 4]. In the past decade, Thouless pumps have been studied in interacting [5–8], non-Abelian [9–12], disorder [13–16] and higher-symmetry protected systems [17–20]. Quasi-periodic systems, in particular, have emerged as a key platform exhibiting exotic phenomena and rich topological transport behavior [21–26].

In Thouless’s original model [1], the potential comprises two sliding commensurate sublattices. Extending this concept to multiple sublattices incommensurate in space and time leads to quasi-periodic structures. Previous studies of quasi-periodic Thouless pumps have mostly focused on boundary-state pumping, where edge modes of lower-dimensional quasi-periodic systems are mapped onto those of higher-dimensional quantum Hall insulators [21–23, 25]. Bulk-state pumping, particularly in systems that are quasi-periodic both spatially and temporally, directly reflects the global topological properties of the system in *spacetime*. However, existing studies along the bulk-state pumping only restrict to systems quasi-periodic in either space [27–30] or time [31]. In periodic systems, pumping can be described by the quantized displacement of the Wannier center over one adiabatic cycle. On the other hand, the study in spacetime quasi-periodic structures is limited due to the infinitely many bands and unbounded periods, which invalidate a conventional Brillouin zone and a well-defined Wannier center displacement.

Moreover, multiple incommensurate modulations induce complicated interband couplings and nontrivial Zener tunneling [32]. The study on bulk-state dynamics and how it encodes the underlying topological invariants is still lacking, e.g., one-dimensional (1D) topological drift velocity was numerically found to be related to, with a high precision, averaged Chern number of populated bands [30], while the underlying mechanism of this empirical rule is unknown. Thus, a systematic framework for spacetime quasi-periodic system beyond purely spatial (or temporal) cases and its extension to higher dimensions remain an open question.

In this Letter, we introduce a general framework for bulk Thouless pumps in continuous models with spacetime quasi-periodicity by simultaneously considering the response of all sliding sublattices. We show that the pumping process, whether periodic or not, is governed by an emergent long-wavelength effective potential. Based on this mechanism, we establish a universal relation between the topological drift velocity and geometry of quasi Brillouin zone (qBZ). Within the commensurate regime, our results yield compact Chern number formula, which extend previous works in two-dimensional (2D) [28] and three dimensional (3D) [29] from a single sliding sublattice to multi-sliding cases. Furthermore, we show that the previously observed averaged Chern-number phenomenon [30] can be quantitatively proven by the effective-potential mechanism. To confirm our proposal, we perform numerical simulations of 1D and 2D continuous moiré-type spacetime quasi-periodic lattices. The results reveal stable, localized, and directional drift of a initially localized state, in excellent agreement with the predicted drift velocity.

Thouless pumps in d -dimensional lattices— We consider the system governed by a dimensionless linear

Gross–Pitaevskii (or Schrödinger) equation,

$$i\frac{\partial}{\partial t}\Psi = -\frac{1}{2}\nabla^2\Psi + V(\mathbf{r},t)\Psi. \quad (1)$$

To analyze the band structure of the system, we define the instantaneous eigenstates $\psi_{n,\mathbf{k}}(x,t)$ and eigenenergies $E_{n,\mathbf{k}}(t)$: $H(\mathbf{r},t)\psi_{n,\mathbf{k}}(\mathbf{r},t) = E_{n,\mathbf{k}}(t)\psi_{n,\mathbf{k}}(\mathbf{r},t)$. Suppose the potential can be split into several sliding sublattices:

$$V(\mathbf{r},t) = \sum V_m \exp[i(\mathbf{b}_m \cdot \mathbf{r} - \phi_m t)] + \text{h.c.} \quad (2)$$

In the nearly-free-electron (NFE) approximation, integer linear combinations of the reciprocal vectors determine a set of Bragg vectors, $\mathbf{G} = \sum_m n_m \mathbf{b}_m$, where $n_m \in \mathbb{Z}$ indicate the order of perturbation [33]. Each Bragg vector \mathbf{G} corresponds to a Bragg plane, which is the perpendicular bisector of \mathbf{G} in momentum space. A Bragg gap opens at the Bragg plane under a generic perturbation. These Bragg planes form a network that provides a geometric partition of the momentum space. Each qBZ is defined as the region associated with a specific isolated group of energy bands, whose boundaries coincide with the Bragg planes corresponding to the upper and lower energy gaps of that group [28, 29, 34, 35], as illustrated in Fig. 1(a). One can express the area of the qBZ as

$$S_{qBZ} = \sum_{\alpha=\{\alpha_1,\alpha_2,\dots,\alpha_d\}} \nu_{\alpha_1,\alpha_2,\dots,\alpha_d} S_{\alpha_1,\alpha_2,\dots,\alpha_d}, \quad (3)$$

where $S_{\alpha_1,\alpha_2,\dots,\alpha_d} \equiv \star(\mathbf{b}_{\alpha_1} \wedge \mathbf{b}_{\alpha_2} \wedge \dots \wedge \mathbf{b}_{\alpha_d})$, with \star the Hodge star and \wedge the exterior product. Each S_α corresponds to a fundamental Brillouin zone spanned by the selected set of $\{\mathbf{b}_{\alpha_1}, \mathbf{b}_{\alpha_2}, \dots, \mathbf{b}_{\alpha_d}\}$. Here α denotes a d -element subset such that $\{\mathbf{b}_{\alpha_1}, \mathbf{b}_{\alpha_2}, \dots, \mathbf{b}_{\alpha_d}\} \subset \{\mathbf{b}_m\}$, where the set $\{\mathbf{b}_m\}$ contain all wave vectors in Eq. (2), and the summation \sum_α runs over all such subsets. For brevity, we write $S_{qBZ} = \sum_\alpha \nu_\alpha S_\alpha$. If the number of vectors in $\{\mathbf{b}_m\}$ is K , there are C_K^d possible subsets α . Each band group can be labeled by the C_K^d integers $\{\nu_\alpha\}$, which correspond to higher-order Chern numbers in electromagnetic responses [28, 29, 36]. For a particular gap,

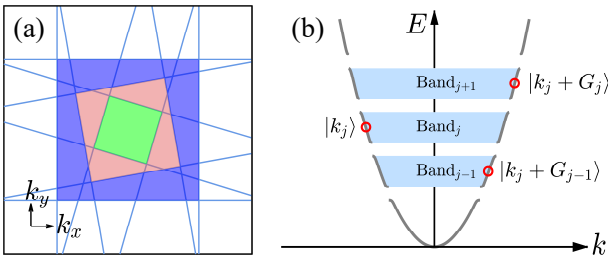


FIG. 1. (a) Bragg planes of a 2D quasi-periodic lattice are shown as blue lines, and three qBZs are filled with different colors. (b) Band structure near Band_j in the nearly-free-electron approximation, with red circles marking the positions of three unperturbed plane-wave states.

the associated qBZ is obtained as the cumulative sum of the qBZs of all band groups lying below that gap, so the gap can also associate with a C_K^d -element set $\{\nu_\alpha\}$, as a gap-labelling [28, 29, 37, 38].

If a band group is fully occupied, the corresponding charge density is $n_e = S_{qBZ}/(2\pi)^d$. For sufficiently small $\{\phi_m\}$, the electrons evolve adiabatically within this band group, generating a current density \mathbf{J} . Consider an infinitesimal change for each sublattices: $\mathbf{b}_m \rightarrow \mathbf{b}_m + \phi_m \delta \mathbf{b}$. In regions far from the origin, the spatial phase shift $\delta \mathbf{b}_m \cdot \mathbf{r}$ varies negligibly within one sublattice period, so that all points in the region experience nearly the same phase change. Such spatial perturbation is equivalent to a time shift $t \rightarrow t - \delta \mathbf{b} \cdot \mathbf{r}$, and both lead to the same physical response. For a region much larger than the sublattice unit cell, the accumulated charge variation thus satisfies

$$\delta n_e V = - \int_{\partial V} \mathbf{J} \cdot d\mathbf{S} \delta t = \int_{\mathbf{r} \in V} \nabla \cdot [\mathbf{J}(\mathbf{r},t) \delta \mathbf{b} \cdot \mathbf{r}] d^d \mathbf{r}, \quad (4)$$

where ∂V is the $(d-1)$ -dimensional boundary surface. \mathbf{J} is assumed uniform in spacetime, so $\mathbf{J} = (2\pi)^{-d} \delta S_{qBZ} / \delta \mathbf{b}$ recalling $n_e = S_{qBZ} / (2\pi)^d$. Substituting the variation into Eq. (3), we obtain

$$\begin{aligned} \frac{\delta S_{qBZ}}{\delta \mathbf{b}} &= \sum_\alpha \nu_\alpha \sum_{m=1}^d \phi_{\alpha_m} \sum_{n=1}^d \mathcal{B}_{\alpha, mn} \mathbf{e}_n \\ &= \frac{1}{2\pi} \sum_\alpha \nu_\alpha S_\alpha \sum_{m=1}^d \phi_{\alpha_m} \mathbf{a}_{\alpha_m}. \end{aligned} \quad (5)$$

Here $\mathbf{e}_1, \mathbf{e}_2, \dots, \mathbf{e}_d$ are unit vector in d -dimensional space. $\mathcal{B}_{\alpha, mn}$ denotes the minor of the matrix B_α , whose matrix element is $(B_\alpha)_{m,n} = \mathbf{b}_{\alpha_m} \cdot \mathbf{e}_n$. And $\{\mathbf{a}_{\alpha_m}\}$ are dual to $\{\mathbf{b}_{\alpha_n}\}$, satisfying $\mathbf{a}_{\alpha_m} \cdot \mathbf{b}_{\alpha_n} = 2\pi \delta_{m,n}$.

Let us specialize results to 1D and 2D. In 1D lattices,

$$S_{qBZ} = \sum_\alpha \nu_\alpha b_\alpha, \quad \frac{\delta S_{qBZ}}{\delta b} = \frac{1}{2\pi} \sum_\alpha \nu_\alpha \phi_\alpha. \quad (6)$$

In 2D lattices,

$$\begin{aligned} S_{qBZ} &= \sum_{\langle \alpha_1, \alpha_2 \rangle} \nu_{\alpha_1, \alpha_2} (\mathbf{b}_{\alpha_1} \times \mathbf{b}_{\alpha_2}) \cdot \mathbf{e}_z, \\ \frac{\delta S_{qBZ}}{\delta \mathbf{b}} &= \sum_{\langle \alpha_1, \alpha_2 \rangle} \nu_{\alpha_1, \alpha_2} (\phi_{\alpha_1} \mathbf{b}_{\alpha_2} - \phi_{\alpha_2} \mathbf{b}_{\alpha_1}) \times \mathbf{e}_z. \end{aligned} \quad (7)$$

Now we use the 1D case to illustrate that, during the pumping process, a localized initial state is governed by an effective potential emerged from interband couplings, and we will derive its explicit form below.

In 1D, each isolated band group Band_j is bounded by two Bragg planes located at $\pm G_{j-1}/2$ and $\pm G_j/2$, corresponding to the Bragg vectors $G_{j-1} = \sum_m \nu_{j-1,m} b_m$ and $G_j = \sum_m \nu_{j,m} b_m$ ($\nu_m \in \mathbb{Z}$), which define the edges of the 1D qBZ. Within the NFE approximation,

we retain only the three plane-wave components with the strongest interband couplings, $|k\rangle$, $|k + G_{j-1}\rangle$, and $|k + G_j\rangle$, with k lying in the interval $(-G_j/2, -G_{j-1}/2)$, as illustrated in Fig. 1(b). Then we define the three basis states as $\rho_1 = |k\rangle$, $\rho_2 = e^{-i\Phi_{j-1}t}|k + G_{j-1}\rangle$, and $\rho_3 = e^{-i\Phi_j t}|k + G_j\rangle$, where $\Phi_{j-1} = \sum_n \nu_{j-1,n} \phi_n$ and $\Phi_j = \sum_n \nu_{j,n} \phi_n$. Such that the reduced Hamiltonian in these basis is real,

$$H = \begin{pmatrix} \varepsilon_0 & \Delta_1 & \Delta_2 \\ \Delta_1 & \varepsilon_0 - \varepsilon_- & \Delta_3 \\ \Delta_2 & \Delta_3 & \varepsilon_0 + \varepsilon_+ \end{pmatrix}, \quad (8)$$

where $\varepsilon_0 = k^2/2$ is the unperturbed energy of the state $|k\rangle$, while $\varepsilon_0 - \varepsilon_-$ and $\varepsilon_0 + \varepsilon_+$ correspond to the unperturbed energies of $|k + G_{j-1}\rangle$ and $|k + G_j\rangle$, respectively. See [40] for the explicit expressions of Δ_1 , Δ_2 , and Δ_3 .

We denote by ψ_j the eigenstate associated with its middle eigenvalue, which corresponds to the perturbed eigenstate of Band _{j} . The momentum separation between adjacent Bragg planes, i.e., $\tilde{G} = G_j - G_{j-1}$, is sufficiently small, so $\Delta_3 \ll \Delta_{1,2}$ and $|\varepsilon_{\pm}| \ll \Delta_{1,2}$. Under this condition, $\psi_j \simeq \mathcal{N}(-\kappa\rho_1 - \Delta_1\rho_2 + \Delta_2\rho_3)$, here \mathcal{N} is the normalization factor and $\kappa \ll \Delta_{1,2}$, with higher-order corrections in [40]. The corresponding probability density becomes

$$\begin{aligned} |\psi_j|^2 &= \mathcal{N}^2[\kappa^2 + \Delta_1^2 + \Delta_2^2 + 2\kappa\Delta_1 \cos(G_{j-1}x - \Phi_{j-1}t) \\ &\quad - 2\kappa\Delta_2 \cos(G_jx - \Phi_j t) - 2\Delta_1\Delta_2 \cos(\tilde{G}x - \tilde{\Phi}t)] \\ &\approx \mathcal{N}^2[\Delta_1^2 + \Delta_2^2 - 2\Delta_1\Delta_2 \cos(\tilde{G}x - \tilde{\Phi}t)]. \end{aligned} \quad (9)$$

Here $\tilde{\Phi} = \Phi_j - \Phi_{j-1}$. Thus, ψ_j is well approximated by the eigenstate of an effective periodic potential

$$\tilde{V}(x, t) = \text{sign}(\Delta_1\Delta_2) \mathcal{V} \cos(\tilde{G}x - \tilde{\Phi}t), \quad (10)$$

where $\mathcal{V} > 0$ is a scaling factor. In the strong potential regime, although many plane-wave components participate in the coupling, the harmonic term $\cos(\tilde{G}x - \tilde{\Phi}t)$, governed by the dominant interband coupling (Band _{$j-1$} and Band _{j}), remains the leading contribution in the eigenstates. Consequently, the eigenstates stays localized near the minima of $\tilde{V}(x, t)$, as shown in the next section of Fig. 2. It thus becomes clear that the drift of the initial state can be viewed from the following perspective: the long-period potential \tilde{V} drives the state to drift with a constant velocity $\mathbf{v} = \tilde{\Phi}/\tilde{G}$, while the effect from other band couplings act as quasi-periodic disorder that help maintain localization. Combining it with Eq. (6), we find that the drift velocity \mathbf{v} is directly linked to the geometry of the qBZ as our main result:

$$\mathbf{v} = \frac{1}{S_{qBZ}} \frac{\delta S_{qBZ}}{\delta \mathbf{b}}, \quad (11)$$

which is expected to remain valid in higher dimensions, as shown in a 2D example later, since the derivation of

the $\tilde{V}(x, t)$ can be naturally generalized to arbitrary dimensions.

Results in commensurate regime— Now suppose the whole system is commensurate in spacetime, with d lattice vectors $\{\mathbf{A}_1, \mathbf{A}_2, \dots, \mathbf{A}_d\}$, d reciprocal lattice vectors $\{\mathbf{B}_1, \mathbf{B}_2, \dots, \mathbf{B}_d\}$ and period T . Then, for each set $\{\mathbf{b}_{\alpha_1}, \dots, \mathbf{b}_{\alpha_d}\}$, the following relation holds: $\mathbf{A}_n = \sum_{m=1}^d r_{\alpha,nm} \mathbf{a}_{\alpha_m}$, $\mathbf{b}_{\alpha_n} = \sum_{m=1}^d r_{\alpha,nm} \mathbf{B}_m$ and $\tau_{\alpha_m} = (\phi_{\alpha_m} T)/2\pi$, where $r_{\alpha,nm}, \tau_{\alpha_m} \in \mathbb{Z}$. Thus the band number N in a particular band group is given by the area of its qBZ divided by that of the first Brillouin zone of the underlying periodic structure,

$$\begin{aligned} N &= \sum_{\langle \alpha \rangle} \nu_{\alpha} \star (\mathbf{b}_{\alpha_1} \wedge \dots \wedge \mathbf{b}_{\alpha_d}) / \star (\mathbf{B}_1 \wedge \dots \wedge \mathbf{B}_d) \\ &= \sum_{\langle \alpha \rangle} \nu_{\alpha} \det(\mathcal{R}_{\alpha}). \end{aligned} \quad (12)$$

The Chern number associated with the direction along \mathbf{A}_m can be expressed as the Berry-curvature flux over the (k_m, t) manifold [39],

$$C_m = \frac{1}{2\pi} \sum_{n \in \text{occupied bands}} \int_{\text{BZ}} d^d \mathbf{k} \int_0^T dt f^{(n)}(\mathbf{k}, t), \quad (13)$$

where $f^{(n)} \equiv \partial_t a_{k_m}^{(n)} - \partial_{k_m} a_t^{(n)}$ and $a_{\mu}^{(n)} \equiv i \langle \psi_{n,k}(\mathbf{r}, t) | \partial_{\mu} | \psi_{n,k}(\mathbf{r}, t) \rangle$ is the Berry connection. It can be alternatively calculated as the total transported charge along \mathbf{A}_m within one pumping cycle [40]:

$$\begin{aligned} C_m &= \star (\mathbf{A}_1 \wedge \dots \wedge \mathbf{A}_{m-1} \wedge J_m \mathbf{e}_{\mathbf{A}_m} \wedge \mathbf{A}_{m+1} \wedge \dots \wedge \mathbf{A}_d) T \\ &= \sum_{\langle \alpha \rangle} \nu_{\alpha} \sum_{n=1}^d \tau_{\alpha_n} \mathcal{R}_{\alpha,nm}. \end{aligned} \quad (14)$$

Here $\mathbf{e}_{\mathbf{A}_m} = \mathbf{A}_m/|\mathbf{A}_m|$, and J_m denotes the magnitude of the component of \mathbf{J} projected onto \mathbf{A}_m . And $\mathcal{R}_{\alpha,nm}$ denotes the minor of the matrix R_{α} whose matrix element is $(R_{\alpha})_{n,m} = r_{\alpha,nm}$.

In 1D lattices,

$$N = \sum_{\alpha} \nu_{\alpha} r_{\alpha}, \quad C = \sum_{\alpha} \nu_{\alpha} \tau_{\alpha}. \quad (15)$$

while in 2D lattices,

$$\begin{aligned} N &= \sum_{\langle \alpha_1, \alpha_2 \rangle} \nu_{\alpha_1, \alpha_2} (t_{\alpha,11} \cdot t_{\alpha,22} - t_{\alpha,12} \cdot t_{\alpha,21}), \\ C_1 &= \sum_{\langle \alpha_1, \alpha_2 \rangle} \nu_{\alpha_1, \alpha_2} (r_{\alpha,22} \tau_{\alpha_1} - r_{\alpha,12} \tau_{\alpha_2}), \\ C_2 &= \sum_{\langle \alpha_1, \alpha_2 \rangle} \nu_{\alpha_1, \alpha_2} (-r_{\alpha,21} \tau_{\alpha_1} + r_{\alpha,11} \tau_{\alpha_2}). \end{aligned} \quad (16)$$

In the commensurate regime, the relation between pumping current and Chern numbers in Eq. (14) can be written as $\mathbf{J} = C_m \mathbf{A}_m / (\Omega T)$, where Ω is the area of the

unit cell. Recall that $n_e = N/\Omega$, the expression of the drift velocity in Eq. (11) then reduces to

$$\mathbf{v} = \sum_{m=1}^d \frac{C_m \mathbf{A}_m}{NT}, \quad (17)$$

as if all bands are “averagedly” populated observed numerically before [30].

Pumping process in quasi-periodic lattices—We numerically simulate the pumping dynamics in 1D and 2D lattices to confirm our general framework and effective-potential proposal.

In 1D, we take the potential as $V_{1D}(x, t) = P_1 \cos(b_1 x - \phi_1 t) + P_2 \cos(b_2 x - \phi_2 t)$. An isolated band group Band_{*j*} is labeled by the Bragg vector $G_j = \nu_{j,1} b_1 + \nu_{j,2} b_2$, $\nu_j \in \mathbb{Z}$. We first consider a periodic case ($b_1 = 2\pi$, $b_2 = \frac{35}{22}\pi$, $\phi_2 = \frac{4}{3}\phi_1$), whose instantaneous band evolution is shown in Fig. 2(a). The lowest five gaps, from low to high energy, are labeled by (1, -1), (2, -2), (-1, 2), (0, 1), and (1, 0). The numerically obtained Chern numbers for each band group are -1, -1, 7, -1, -1, respectively, matching Eq. (15). Figure 2(b) displays effective potentials and Bloch-state densities $|\psi_{n,k=0}(x, t)|^2$ at $\phi_1 t = 2$. $|\psi_{n,k=0}(x, t)|^2$ are all exactly localized near the minima of their effective potentials, confirming their role in governing the adiabatic drift. To demonstrate the pumping process, we introduce spacetime quasi-periodic structure by

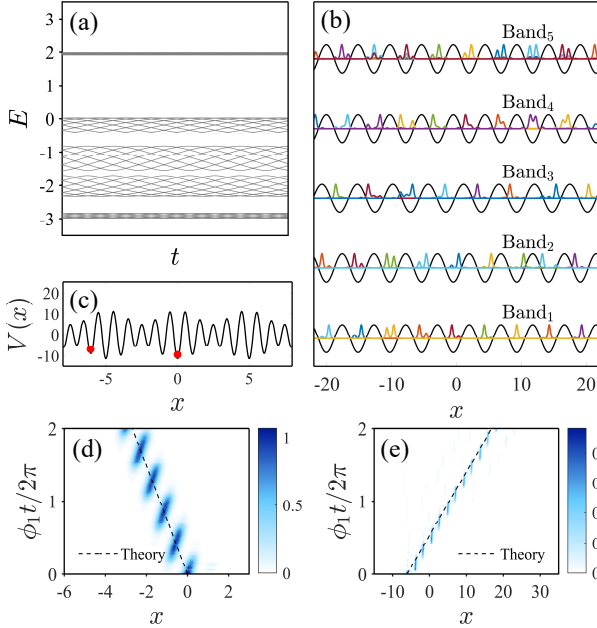


FIG. 2. (a,b) Results of the periodic lattice. (a) Evolution of $E_{n,k=0}(t)$. (b) For each band group, \tilde{V} is plotted in black and $|\psi_{n,k=0}(x)|^2$ of different bands are shown as colored lines. (c) The quasi-periodic potential at $t = 0$ is shown as a black line, with red dots marking two initial excitation positions. (d,e) Time evolutions of $|\Psi(x, t)|^2$ in the quasi-periodic lattice for excitations in Band₁ and Band₃, respectively. In all cases, $\phi_1 = 3\pi \times 10^{-3}$, $P_1 = -8$ and $P_2 = -3.5$.

setting $b_2 = 5$ and $\phi_2 = \frac{4}{\pi}\phi_1$, which shares the same gap labelling as the former periodic one. Localized Gaussian inputs, $\Psi(x, 0) = e^{-x^2/0.17}$ and $\Psi(x, 0) = e^{-(x-6.1)^2/0.17}$, are used to excite Band₁ and Band₃, respectively, as marked in Fig. 2(c). Time evolutions of $|\Psi(x, t)|^2$ shown in Figs. 2(d,e) reveal robust, localized transport with constant velocities in agreement with the theoretical prediction Eq. (11).

We next construct a 2D potential: $V_{2D}(\mathbf{r}, t) = V_1 + V_2$, where $V_i = P_i \cos(\mathbf{b}_{i1} \cdot \mathbf{r} - \phi_i t) + P_i \cos(\mathbf{b}_{i2} \cdot \mathbf{r} - \phi_i t)$, with $i = 1, 2$. Four reciprocal lattice vectors are $\mathbf{b}_{11} = (\beta_1, 0)$, $\mathbf{b}_{12} = (0, \beta_1)$ and $\mathbf{b}_{21} = (\beta_2 \cos \theta, \beta_2 \sin \theta)$, $\mathbf{b}_{22} = (-\beta_2 \sin \theta, \beta_2 \cos \theta)$ illustrated in Fig. 3(a). We first take a periodic structure with parameters $\theta = \arctan(7/24)$, $\beta_1 = 2\pi$, $\beta_2 = \frac{8}{5}\pi$ and $\phi_2 = 4/3$. The instantaneous band evolution is shown in Fig. 3(b). For the lowest isolated band group (Band₁), the Bragg vectors are $\tilde{\mathbf{b}}_1 = \mathbf{b}_{11} - \mathbf{b}_{21}$ and $\tilde{\mathbf{b}}_2 = \mathbf{b}_{12} - \mathbf{b}_{22}$. Two Chern numbers are $C_1 = -5$ and $C_2 = -1$, equal to those calculated from Eq. (16). The associated effective potential is

$$\tilde{V}(\mathbf{r}, t) = -\mathcal{V} \cos(\tilde{\mathbf{b}}_1 \cdot \mathbf{r} - \tilde{\phi}) - \mathcal{V} \cos(\tilde{\mathbf{b}}_2 \cdot \mathbf{r} - \tilde{\phi}), \quad (18)$$

where $\tilde{\phi} = \phi_1 - \phi_2$, and $\mathcal{V} > 0$ is the scaling factor. As shown in Fig. 3(c), the Bloch-state densities of Band₁ at $\phi_1 t = 2$ are strongly localized near the minima of \tilde{V} . Then we set $\beta_2 = 5$, $\theta = 10^\circ$, and $\phi_2 = \frac{4}{\pi}\phi_1$ to make

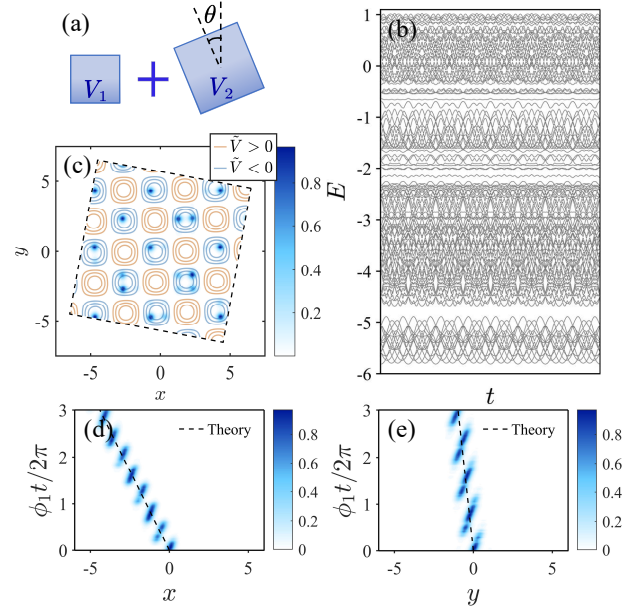


FIG. 3. (a) Schematic of $V_{2D}(\mathbf{r}, t)$. (b,c) Results of the periodic lattice. (a) Evolution of $E_{n,k=0}(t)$. (b) $|\psi_{n,k=0}(r)|^2$ of all bands in the Band₁ are shown in a blue color scale. Contours of $\tilde{V}(\mathbf{r}, t)$ in Eq. (18) are overlaid. The dashed line indicates the boundary of one unit cell. (d,e) Time evolutions of $|\Psi(x, y, t)|^2$ in the quasi-periodic lattice when Band₁ is excited; (d) and (e) show the projections along x and y , respectively, by taking $\max(|\Psi(x, y, t)|^2)$ over the other coordinate. In all cases, $\phi_1 = 3\pi \times 10^{-3}$, $P_1 = -8$ and $P_2 = -3.5$.

$V_{2D}(\mathbf{r}, t)$ be spacetime quasi-periodic. From Eq. (18), the drift velocity should be $\mathbf{v}_{2D} = \dot{\phi}(\tilde{\mathbf{b}}_1 + \tilde{\mathbf{b}}_2)/(\tilde{\mathbf{b}}_1 \times \tilde{\mathbf{b}}_2) \cdot \mathbf{e}_z$, the same as our prediction Eq. (11). We set $\Psi(\mathbf{r}, t) = \exp[-(x^2 + y^2)/0.17]$ to excite Band₁, and the evolution of $|\Psi(\mathbf{r}, t)|^2$ is shown in Fig. 3(d) and (e). The results show excellent consistency with our proposal.

Conclusion— We have developed a unifying framework for Thouless pumps continuous models with spacetime quasi-periodicity. We show that the evolution of a localized state is governed by a long-wavelength effective potential emerging from interband couplings. As a consequence, we establish a universal relation between the topological drift velocity and the geometric structure of the qBZ. Numerical simulations in 1D and 2D quasi-periodic lattices confirm the theory and its dynamical picture, revealing stable, localized and directional drift of a initially localized state. Our approach of analyzing the dynamics from the perspective of an effective potential may offer inspiration for studying interacting Thouless pumps involving multiple bands as future interest.

Acknowledgements.— The authors thank Fangwei Ye for useful discussions. The work of Y. Y. was supported by the National Key Research and Development Program of China (Grant No. 2024YFA1408303), the National Natural Science Foundation of China (Grants No. 12474157 and No. 12447103), the sponsorship from Yangyang Development Fund, and Xiaomi Young Scholars Program.

* smartyao@sjtu.edu.cn; Corresponding author.

- [1] D. J. Thouless, *Phys. Rev. B* **27**, 6083 (1983).
- [2] D. J. Thouless, M. Kohmoto, M. P. Nightingale, and M. den Nijs, *Phys. Rev. Lett.* **49**, 405 (1982).
- [3] Q. Niu, *Phys. Rev. Lett.* **64**, 1812 (1990).
- [4] J. P. Pekola, O.-P. Saira, V. F. Maisi, A. Kemppinen, M. Möttönen, Y. A. Pashkin, and D. V. Averin, *Rev. Mod. Phys.* **85**, 1421 (2013).
- [5] M. Jürgensen, S. Mukherjee, and M. C. Rechtsman, *Nature* **596**, 63 (2021).
- [6] Q. Fu, P. Wang, Y. V. Kartashov, V. V. Konotop, and F. Ye, *Phys. Rev. Lett.* **128**, 154101 (2022).
- [7] M. Jürgensen, J. Steiner, G. Refael, and M. C. Rechtsman, *Phys. Rev. Lett.* **135**, 166601 (2025).
- [8] Y.-L. Tao, Y. Zhang, and Y. Xu, *Phys. Rev. Lett.* **135**, 097202 (2025).
- [9] O. You, S. Liang, B. Xie, W. Gao, W. Ye, J. Zhu, and S. Zhang, *Phys. Rev. Lett.* **128**, 244302 (2022).
- [10] Y.-K. Sun, X.-L. Zhang, F. Yu, Z.-N. Tian, Q.-D. Chen, and H.-B. Sun, *Nature Physics* **18**, 1080 (2022).
- [11] Y.-K. Sun, Z.-L. Shan, Z.-N. Tian, Q.-D. Chen, and X.-L. Zhang, *Nature Communications* **15**, 9311 (2024).
- [12] V. Brosco, L. Pilozi, R. Fazio, and C. Conti, *Phys. Rev. A* **103**, 063518 (2021).
- [13] A. L. C. Hayward, E. Bertok, U. Schneider, and F. Heidrich-Meisner, *Phys. Rev. A* **103**, 043310 (2021).
- [14] S. Hu, Y. Ke, and C. Lee, *Phys. Rev. A* **101**, 052323 (2020).
- [15] M. Ippoliti and R. N. Bhatt, *Phys. Rev. Lett.* **124**, 086602 (2020).
- [16] Y. Liu, Y.-R. Zhang, Y.-H. Shi, T. Liu, C. Lu, Y.-Y. Wang, H. Li, T.-M. Li, C.-L. Deng, S.-Y. Zhou, *et al.*, *Nature Communications* **16**, 108 (2025).
- [17] B. Kang, K. Shiozaki, and G. Y. Cho, *Phys. Rev. B* **100**, 245134 (2019).
- [18] I. Petrides and O. Zilberberg, *Phys. Rev. Res.* **2**, 022049 (2020).
- [19] J. F. Wienand, F. Horn, M. Aidelsburger, J. Bibo, and F. Grusdt, *Phys. Rev. Lett.* **128**, 246602 (2022).
- [20] H. Araki, T. Mizoguchi, and Y. Hatsugai, *Phys. Rev. Res.* **2**, 012009 (2020).
- [21] Y. E. Kraus, Y. Lahini, Z. Ringel, M. Verbin, and O. Zilberberg, *Phys. Rev. Lett.* **109**, 106402 (2012).
- [22] O. Zilberberg, S. Huang, J. Guglielmon, M. Wang, K. P. Chen, Y. E. Kraus, and M. C. Rechtsman, *Nature* **553**, 59 (2018).
- [23] M. Lohse, C. Schweizer, H. M. Price, O. Zilberberg, and I. Bloch, *Nature* **553**, 55 (2018).
- [24] W. Cheng, E. Prodan, and C. Prodan, *Phys. Rev. Lett.* **125**, 224301 (2020).
- [25] M. Verbin, O. Zilberberg, Y. Lahini, Y. E. Kraus, and Y. Silberberg, *Phys. Rev. B* **91**, 064201 (2015).
- [26] S. Nakajima, N. Takei, K. Sakuma, Y. Kuno, P. Marra, and Y. Takahashi, *Nature Physics* **17**, 844 (2021).
- [27] P. Marra and M. Nitta, *Phys. Rev. Res.* **2**, 042035 (2020).
- [28] M. Koshino and H. Oka, *Phys. Rev. Res.* **4**, 013028 (2022).
- [29] K. Yamamoto and M. Koshino, *Phys. Rev. B* **105**, 115410 (2022).
- [30] K. Yang, Q. Fu, H. C. Prates, P. Wang, Y. V. Kartashov, V. V. Konotop, and F. Ye, *Proceedings of the National Academy of Sciences* **121**, e2411793121 (2024).
- [31] R. Peng, K. Yang, Q. Fu, Y. Chen, P. Wang, Y. V. Kartashov, V. V. Konotop, and F. Ye, *ELight* **5**, 16 (2025).
- [32] R. Citro and M. Aidelsburger, *Nature Reviews Physics* **5**, 87 (2023).
- [33] Q. Niu, *Phys. Rev. B* **34**, 5093 (1986).
- [34] M. Yoshii, S. Kitamura, and T. Morimoto, *Phys. Rev. B* **107**, 064201 (2023).
- [35] M. K. Jat, P. Tiwari, R. Bajaj, I. Shitut, S. Mandal, K. Watanabe, T. Taniguchi, H. Krishnamurthy, M. Jain, and A. Bid, *Nature Communications* **15**, 2335 (2024).
- [36] I. Petrides, H. M. Price, and O. Zilberberg, *Phys. Rev. B* **98**, 125431 (2018).
- [37] J. Bellissard, R. Benedetti, and J.-M. Gambaudo, *Communications in Mathematical Physics* **261**, 1 (2006).
- [38] J. Kellendonk, *Journal of Mathematical Physics* **64** (2023).
- [39] D. Vanderbilt, *Berry phases in electronic structure theory: electric polarization, orbital magnetization and topological insulators* (Cambridge University Press, 2018).
- [40] See Supplemental Materials.
- [41] J. J. Sakurai and J. Napolitano, *Modern quantum mechanics* (Cambridge University Press, 2020).

SUPPLEMENTAL MATERIALS

DETAILED CALCULATIONS OF SEVERAL QUANTITIES

In this section, we present the full derivation of the variation $\frac{\delta S_{BZ}}{\delta \mathbf{b}}$ and the Chern numbers C_m . We first perform the variation $\mathbf{b}_m \rightarrow \mathbf{b}_m + \phi_m \delta \mathbf{b}$ to calculate the response of S_{qBZ} . Recall that $S_{qBZ} = \sum_{\alpha} \nu_{\alpha} S_{\alpha}$, where $S_{\alpha} = \star(\mathbf{b}_{\alpha_1} \wedge \mathbf{b}_{\alpha_2} \wedge \cdots \wedge \mathbf{b}_{\alpha_d})$, so

$$\begin{aligned} \delta S_{qBZ} &= \sum_{\alpha} \nu_{\alpha} \star [(\mathbf{b}_{\alpha_1} + \phi_{\alpha_1} \delta \mathbf{b}) \wedge \cdots \wedge (\mathbf{b}_{\alpha_d} + \phi_{\alpha_d} \delta \mathbf{b})] - S_{qBZ} \\ &= \sum_{\alpha} \nu_{\alpha} \sum_{m=1}^d (-1)^{m-1} \phi_{\alpha_m} \delta \mathbf{b} \star (\mathbf{b}_{\alpha_1} \wedge \cdots \wedge \mathbf{b}_{\alpha_{m-1}} \wedge \mathbf{b}_{\alpha_{m+1}} \wedge \cdots \wedge \mathbf{b}_{\alpha_d}). \end{aligned} \quad (19)$$

Consequently,

$$\begin{aligned} \frac{\delta S_{BZ}}{\delta \mathbf{b}} &= \sum_{\alpha} \nu_{\alpha} \sum_{m=1}^d \phi_{\alpha_m} \det \begin{pmatrix} b_{\alpha_1}^1 & b_{\alpha_1}^2 & \cdots & b_{\alpha_1}^d \\ \vdots & \vdots & & \vdots \\ b_{\alpha_{m-1}}^1 & b_{\alpha_{m-1}}^2 & \cdots & b_{\alpha_{m-1}}^d \\ \mathbf{e}_1 & \mathbf{e}_2 & \cdots & \mathbf{e}_d \\ b_{\alpha_{m+1}}^1 & b_{\alpha_{m+1}}^2 & \cdots & b_{\alpha_{m+1}}^d \\ \vdots & \vdots & & \vdots \\ b_{\alpha_d}^1 & b_{\alpha_d}^2 & \cdots & b_{\alpha_d}^d \end{pmatrix} \\ &= \sum_{\alpha} \nu_{\alpha} \sum_{m=1}^d \phi_{\alpha_m} \sum_{n=1}^d \mathcal{B}_{\alpha, mn} \mathbf{e}_n \end{aligned} \quad (20)$$

$\mathbf{e}_1, \mathbf{e}_2, \dots, \mathbf{e}_d$ are unit vectors in d-dimensional space, $\mathcal{B}_{\alpha, mn}$ denotes the minor of the matrix B_{α} , whose matrix element is $(B_{\alpha})_{m,n} = \mathbf{b}_{\alpha_m} \cdot \mathbf{e}_n$. We now introduce a set of dual lattice vectors $\{\mathbf{a}_{\alpha_m}\}$ via

$$(-1)^{m-1} \star (\mathbf{b}_{\alpha_1} \wedge \cdots \wedge \mathbf{b}_{\alpha_{m-1}} \wedge \mathbf{b}_{\alpha_{m+1}} \wedge \cdots \wedge \mathbf{b}_{\alpha_d}) = \frac{1}{2\pi} S_{\alpha_1, \alpha_2, \dots, \alpha_d} \mathbf{a}_{\alpha_m} \quad (21)$$

These dual vectors satisfy $\mathbf{a}_{\alpha_m} \cdot \mathbf{b}_{\alpha_n} = 2\pi \delta_{m,n}$, then we obtain

$$\frac{\delta S_{BZ}}{\delta \mathbf{b}} = \frac{1}{2\pi} \sum_{\alpha} \nu_{\alpha} S_{\alpha} \sum_{m=1}^d \phi_{\alpha_m} \mathbf{a}_{\alpha_m}. \quad (22)$$

Now we work in the commensurate regime and use the same notation $\mathbf{A}_n = \sum_{m=1}^d r_{\alpha, nm} \mathbf{a}_{\alpha_m}$, $\mathbf{b}_{\alpha_n} = \sum_{m=1}^d r_{\alpha, nm} \mathbf{B}_m$ and $\tau_{\alpha_m} = (\phi_{\alpha_m} T)/2\pi$ as in the main text. $\{\mathbf{A}_n\}$ and $\{\mathbf{B}_m\}$ denote the lattice vectors and their reciprocal counterparts, respectively. T is the pumping period. The Chern number C_m of a Thouless pump is defined as the total amount of charge transported along a given direction \mathbf{A}_m during one pumping cycle,

$$\begin{aligned} C_m &= \star(A_1 \wedge \cdots \wedge \mathbf{A}_{m-1} \wedge J_m \mathbf{e}_{A_m} \wedge \mathbf{A}_{m+1} \wedge \cdots \wedge A_d) T \\ &= (-1)^{m-1} \frac{1}{2\pi} (\mathbf{J} \cdot \mathbf{B}_m) \mathbf{A}_m \cdot \star(\mathbf{A}_1 \wedge \mathbf{A}_2 \wedge \cdots \wedge \mathbf{A}_d) T \\ &= \frac{\Omega}{2\pi} \mathbf{J} \cdot \mathbf{B}_m T. \end{aligned} \quad (23)$$

Here $\mathbf{e}_{A_m} = \mathbf{A}_m / |\mathbf{A}_m|$ and J_m denotes the magnitude of the component of \mathbf{J} projected onto \mathbf{e}_{A_m} . Ω is the unit cell

volume. Using the relation $\mathbf{J} = (2\pi)^{-d} \delta S_{BZ} / \delta \mathbf{b}$ and substituting Eq. (19) into Eq. (23), we obtain

$$\begin{aligned}
C_m &= \frac{\Omega}{(2\pi)^d} \sum_{\alpha} \nu_{\alpha} \sum_{n=1}^d \tau_{\alpha_n} \star (\mathbf{b}_{\alpha_1} \wedge \cdots \wedge \mathbf{b}_{\alpha_{n-1}} \wedge \mathbf{B}_m \wedge \mathbf{b}_{\alpha_{n+1}} \wedge \cdots \wedge \mathbf{b}_{\alpha_d}) \\
&= \sum_{\alpha} \nu_{\alpha} \sum_{n=1}^d \tau_{\alpha_n} \det \begin{pmatrix} r_{\alpha,1,1} & \cdots & r_{\alpha,1,m-1} & r_{\alpha,1,m} & r_{\alpha,1,m+1} & \cdots & r_{\alpha,1,d} \\ \vdots & & & & & & \vdots \\ r_{\alpha,n-1,1} & \cdots & r_{\alpha,n-1,m-1} & r_{\alpha,n-1,m} & r_{\alpha,n-1,m+1} & \cdots & r_{\alpha,n-1,d} \\ 0 & \cdots & 0 & 1 & 0 & \cdots & 0 \\ r_{\alpha,n+1,1} & \cdots & r_{\alpha,n+1,m-1} & r_{\alpha,n+1,m} & r_{\alpha,n+1,m+1} & \cdots & r_{\alpha,n+1,d} \\ \vdots & & & & & & \vdots \\ r_{\alpha,d,1} & \cdots & r_{\alpha,d,m-1} & r_{\alpha,d,m} & r_{\alpha,d,m+1} & \cdots & r_{\alpha,d,d} \end{pmatrix} \\
&= \sum_{\langle \alpha \rangle} \nu_{\alpha} \sum_{n=1}^d \tau_{\alpha_n} \mathcal{R}_{\alpha,nm}.
\end{aligned} \tag{24}$$

$\mathcal{R}_{\alpha,nm}$ denotes the minor of the matrix R_{α} , whose matrix element is $(R_{\alpha})_{n,m} = r_{\alpha,nm}$.

EFFECTIVE HAMILTONIAN AND EFFECTIVE POTENTIAL

In this section, we construct the effective Hamiltonian matrix and derive the corresponding effective potential under the NFE approximation in 1D. We consider the j -th isolated group of bands (denote as Band $_j$), in which one of the unperturbed eigenstates is $\psi_j^0 = |k\rangle = \frac{1}{\sqrt{L}} \exp(ikx)$. The Dyson-Schwinger equation [41] leads to an effective Hamiltonian acting on the low-energy subspace,

$$\begin{aligned}
H_{\text{eff}}(E) &= PHP + PHQ(E - QHQ)^{-1}QHP, \\
&= PH_0P + \sum_{n=0}^{\infty} PV(Q \frac{1}{E - H_0} QV)^n P.
\end{aligned} \tag{25}$$

where P projects onto the selected subspace that we care about, and $Q = 1 - P$ projects onto the remaining states. The pertubated eigenfunction is $H_{\text{eff}}(E)\psi_j = E\psi_j$, where we have restricted ψ_j in the selected subspace. The expansion occurs when there exist energy separation between P and Q . In our model, the time-dependent potential takes the form $V(x, t) = \sum_m V_m e^{i(b_m x - 2\pi \phi_m t)} + \text{c.c.}$. So the two unpertubated states $|k_a\rangle = \frac{1}{\sqrt{L}} \exp(ik_a x)$ and $|k_\beta\rangle = \frac{1}{\sqrt{L}} \exp(ik_\beta x)$ can be coupld only when $k_\beta - k_\alpha = \sum \nu_m b_m$, $\nu_m \in \mathbb{Z}$. Their coupling coefficient is

$$\langle k_\alpha | H_{\text{eff}}(E) | k_\beta \rangle = \sum_{p=(p_1, \dots, p_l)} \frac{\prod_{j=1}^l V_{p_j} \exp(-i\phi_{p_j} t)}{\prod_{j=1}^{l-1} E - \frac{1}{2}(k_\alpha + \sum_{s=1}^j b_{p_s})^2}. \tag{26}$$

Here $b_{p_1, 2, \dots, l} \in \{b_m\}$, and the summation runs over all possible scattering paths $p = \{p_1, \dots, p_l\}$ that connect the two momenta k_α and k_β , satisfying $\sum_{s=1}^l b_{p_s} = k_\beta - k_\alpha$. So the accumulated phase is the same for each path p , i.e., $\sum_{j=1}^l \phi_{p_j} t = \sum_m \nu_m \phi_m t$. We can thus denote the the coupling coefficient as $\langle k_\alpha | H_{\text{eff}}(E) | k_\beta \rangle = e^{-i \sum_m \nu_m \phi_m t} \Delta_{\alpha\beta}$, where $\Delta_{\alpha\beta} \in \mathbb{R}$.

In 1D, Band $_j$ is bounded by two Bragg planes located at $\pm G_{j-1}/2$ and $\pm G_j/2$, corresponding respectively to the lower Gap $_{j-1}$ and the upper Gap $_j$, where $G_j = \sum \nu_{j,m} b_m$ and $G_{j-1} = \sum \nu_{j-1,m} b_m$. We set $k \in (-G_j/2, -G_{j-1}/2)$ and retain only the two states that couple most strongly to $|k\rangle$, namely $|k + G_{j-1}\rangle$ in Band $_{j-1}$ and $|k + G_j\rangle$ in Band $_{j+1}$. So

$$P = |k\rangle\langle k| + |k + G_{j-1}\rangle\langle k + G_{j-1}| + |k + G_j\rangle\langle k + G_j|. \tag{27}$$

In the self-consistent equation Eq. (25), the difference between the exact eigenenergy E and the unpertubated energy $\epsilon_0 = \frac{1}{2}k^2$ contributes only to higher-order corrections. So we set $E = \epsilon_0$ as an approximate value when constructing the expression of H_{eff} . We redefine the three basis states as $|\rho_1\rangle = |k\rangle$, $|\rho_2\rangle = e^{-i\Phi_{i-1}t} |k + G_{j-1}\rangle$, and $|\rho_3\rangle = e^{-i\Phi_{i+1}t} |k + G_j\rangle$,

where the phase factors are given by $\Phi_{j-1} = \sum_m \nu_{j-1,m} \phi_m$ and $\Phi_j = \sum_m \nu_{j,m} \phi_m$. Under such choice, all matrix elements of H are real. The effective Hamiltonian matrix takes the form

$$H_{\text{eff}} = \varepsilon_0 + \begin{pmatrix} 0 & \Delta_1 & \Delta_2 \\ \Delta_1 & \varepsilon_- & \Delta_3 \\ \Delta_2 & \Delta_3 & \varepsilon_+ \end{pmatrix}, \quad \begin{cases} \Delta_1 = e^{i\Phi_{j-1}t} \langle k | H_{\text{eff}} | k + G_{j-1} \rangle, \\ \Delta_2 = e^{i\Phi_j t} \langle k | H_{\text{eff}} | k + G_j \rangle, \\ \Delta_3 = e^{i(\Phi_j - \Phi_{j-1})t} \langle k + G_{j-1} | H_{\text{eff}} | k + G_j \rangle. \end{cases} \quad (28)$$

Here $\varepsilon_0 + \varepsilon_- = \frac{1}{2}(k + G_{j-1})^2$ and $\varepsilon_0 + \varepsilon_+ = \frac{1}{2}(k + G_j)^2$.

Let $\cos(\theta) = \Delta_1/R$ and $\sin(\theta) = \Delta_2/R$, here $R = \sqrt{\Delta_1^2 + \Delta_2^2}$. We perform a linear transformation: $|\rho'_2\rangle = \cos(\theta)|\rho_2\rangle + \sin(\theta)|\rho_3\rangle$, $|\rho'_3\rangle = -\sin(\theta)|\rho_2\rangle + \cos(\theta)|\rho_3\rangle$. The transformed Hamiltonian matrix takes the following form:

$$H'_{\text{eff}} = \varepsilon_0 + \begin{pmatrix} 0 & R & 0 \\ R & \varepsilon'_- & \Delta'_3 \\ 0 & \Delta'_3 & \varepsilon'_+ \end{pmatrix}, \quad \begin{cases} \varepsilon'_- = \frac{\Delta_1^2 \varepsilon_- + \Delta_2^2 \varepsilon_+ + 2\Delta_1 \Delta_2 \Delta_3}{R^2}, \\ \varepsilon'_+ = \frac{\Delta_2^2 \varepsilon_- + \Delta_1^2 \varepsilon_+ - 2\Delta_1 \Delta_2 \Delta_3}{R^2}, \\ \Delta'_3 = \frac{(\Delta_1^2 - \Delta_2^2) \Delta_3 + \Delta_1 \Delta_2 (\varepsilon_+ - \varepsilon_-)}{R^2}. \end{cases} \quad (29)$$

Since $G_j - G_{j-1}$ represents the separation between two adjacent gaps in k -space and is relatively small, a sufficiently strong lattice potential may make $|\varepsilon_{\pm}|$ much smaller than $\Delta_{1,2}$. Moreover, the coupling Δ_3 usually originates from longer scattering paths than $\Delta_{1,2}$, so Δ_3 is also much smaller than $\Delta_{1,2}$. As a result, $|\varepsilon'_{\pm}|$ and Δ'_3 are much smaller than R . Therefore, H'_{eff} has two eigenvalues with magnitudes around $\varepsilon_0 \pm R$, and one intermediate eigenvalue close to $\varepsilon_0 + \varepsilon'_+$, which corresponds to the eigenenergy of ψ_j . We set the eigenvalue as $\lambda = \varepsilon_0 + \varepsilon'_+ + \xi$. Neglecting higher-order terms of ξ in the eigenvalue equation yields

$$\xi \approx -\frac{(\Delta'_3)^2}{D}, \quad D = \frac{R^2}{\varepsilon'_+} + \varepsilon'_- - \varepsilon'_+. \quad (30)$$

Based on this eigenvalue λ , we obtain the corresponding eigenstate and express it in the original basis $\{|\rho_1\rangle, |\rho_2\rangle, |\rho_3\rangle\}$ as

$$\begin{aligned} |\psi_j\rangle &\approx \mathcal{N}(a|\rho_1\rangle + b|\rho_2\rangle - c|\rho_3\rangle), \\ a &= \frac{\Delta'_3}{1 - \varepsilon'_+(\varepsilon'_+ - \varepsilon'_-)/R^2}, \\ b &= \Delta_2 + \frac{\Delta'_3 \Delta_1}{D}, \\ c &= \Delta_1 - \frac{\Delta'_3 \Delta_2}{D}. \end{aligned} \quad (31)$$

where \mathcal{N} is the normalization factor. So

$$\begin{aligned} |\psi_j|^2 &= \mathcal{N}^2[a^2 + b^2 + c^2 + 2ab \cdot \cos(G_{j-1}x - \Phi_{j-1}t) \\ &\quad - 2ac \cdot \cos(G_j x - \Phi_j t) - 2bc \cdot \cos(\tilde{G}x - \tilde{\Phi}t)]. \end{aligned} \quad (32)$$

Here $\tilde{G} = G_j - G_{j-1}$, $\tilde{\Phi} = \Phi_j - \Phi_{j-1}$. a is much smaller than b, c , so ψ_j as the eigenstate of Band $_j$ is well approximated by the first-band eigenstate of the effective potential

$$\tilde{V}(x, t) = \text{sign}[(\Delta_2 + \frac{\Delta'_3 \Delta_1}{D})(\Delta_1 - \frac{\Delta'_3 \Delta_2}{D})] \cdot \mathcal{V} \cos(\tilde{G}x - \tilde{\Phi}t), \quad (33)$$

$\mathcal{V} > 0$ is the scaling factor. Under a wide range of parametres, $\text{sign}(bc) \equiv \text{sign}(\Delta_1 \Delta_2)$. If Band $_j$ is bounded by extremely higher order perturbations, the difference in magnitude between $\varepsilon_{\pm}, \Delta_3$ and $\Delta_{1,2}$ will decrease. In very extreme cases, this may lead to $\text{sign}(bc) \equiv -\text{sign}(\Delta_1 \Delta_2)$.